



Ozone-Gravity Wave Interaction in the Upper Stratosphere/Lower Mesosphere

Axel Gabriel

25 Leibniz-Institute of Atmospheric Physics at the University Rostock e.V. (IAP)

Correspondence to: Axel Gabriel (gabriel@iap-kborn.de)

Abstract. The increase in amplitudes of upward propagating gravity waves (GWs) with height due to decreasing density is usually described by exponential growth; however, recent measurements detected a much stronger increase in gravity wave potential energy density (GWPED) during daylight than night-time (increase by a factor of about 4 to 8 between middle
30 stratosphere and upper mesosphere), which is not well understood up to now. This paper suggests that ozone-gravity wave interaction in the upper stratosphere/lower mesosphere is largely responsible for this phenomenon. The coupling between ozone-photochemistry and temperature is particularly strong in the upper stratosphere where the time-mean ozone mixing ratio is decreasing with height; therefore, an initial uplift of an air parcel must lead to a local increase in ozone and in the heating rate compared to the environment, and, hence, to an amplification of the initial uplift. Standard solutions of upward
35 propagating GWs with linear ozone-temperature coupling are formulated suggesting local amplitude amplifications during daylight of 5 to 15% for low-frequency GWs (periods ≥ 4 hours), as a function of the intrinsic frequency which decreases if ozone-temperature coupling is included. Subsequently, for horizontal wavelengths larger than 500 km and vertical wavelengths smaller than 5 km, the cumulative amplification during the upward level-by-level propagation leads to much stronger amplitudes in the GW perturbations (factor of about 1.5 to 3) and in the GWPED (factor of about 3 to 9) at upper
40 mesospheric altitudes. The results open a new viewpoint for improving general circulation models with resolved or parameterized GWs.

1 Introduction

Atmospheric gravity waves (GWs), with horizontal wavelengths of 100 km to 2000 km, are produced in the troposphere and propagate vertically through the stratosphere and mesosphere, where gravity wave breaking processes are an important
45 driver of the middle atmospheric circulation (e.g., Andrews et al., 1986; Fritts and Alexander, 2003). Usually, upward propagating GWs are described by sinusoidal wave perturbations in a slowly varying background flow with an exponentially growing amplitude with height due to decreasing density ($\sim e^{z/2H}$, where H is the scale height). However, recent Lidar measurements detected much stronger, over-exponentially growing GW amplitudes during daylight than nighttime, or polar summer than winter, which is not well understood up to now (Kaifler et al., 2015; Baumgarten et al., 2017, 2018). The aim
50 of the present paper is to examine whether ozone-gravity wave interaction can principally produce such an amplification.



Kaifler et al. (2015) derived GW temperature fluctuations and monthly mean GW potential energy density (GWPED) from full-day Lidar temperature measurements at southern polar latitudes (69°S, 78°E). One result was that the GWPED of the middle stratosphere (30-40 km) is generally smaller during polar summer than winter, but that the rate of increase in GWPED between middle stratosphere and upper mesosphere (85-95 km) is stronger during polar summer than winter by a factor of up to ~8 (increase from ~40 J kg⁻¹ to ~65 J kg⁻¹ during July, and from ~8 J kg⁻¹ to ~104 J kg⁻¹ during January), which cannot be explained by exponential growth and GW filtering processes only. Baumgarten et al. (2017) derived the GWPED from full-day Lidar temperature measurements at northern mid-latitudes (54°N, 12°E), and found much stronger values at 60 km compared to 35 km for full-day than night-time observations during summer (factor of more than ~2) but less pronounced differences during winter. Subsequently, assuming roughly a half-day-half-night relation of the related effects during mid-latitude summer months, the increase of the GWPED amplitudes might be stronger during daylight than night-time by a factor of up to ~4. In addition, full-day observations of Baumgarten et al. (2018) during May 2016 showed pronounced GW activity particularly at altitudes between 42 km and 50 km. Kaifler et al. (2015) assumed that specific GWs with large phase speeds not filtered by the zonal wind could be the reason of the summer maximum. Chen et al. (2019) suggested that specific GWs generated by convection and propagating towards polar latitudes could contribute to the unusual strong GWPED during summer. However, the much stronger increase of the GWPED with height during polar summer than winter, or during daylight than night-time, is not well understood up to now.

The coupling of temperature and ozone is particularly strong in the upper stratosphere due to the short photochemical lifetime of ozone (e.g., Brasseur and Solomon, 1995). Linear relationships for a change in the heating rate due to a change in ozone, and a change in photochemistry due to a change in temperature, were derived from basic theory or satellite observations, and have been introduced in standard equations of stratospheric dynamics to examine the effects on the stratospheric circulation, planetary-scale wave patterns and equatorial Kelvin waves (Dickinson, 1973; Douglass et al., 1985; Froidevaux et al., 1989; Cordero et al. 1998, 2000; Nathan et al., 2007; Ward et al., 2010; Gabriel et al., 2011a). Large-scale ozone-dynamic coupling processes show also significant effects in numerical weather prediction or general circulation models (Cariolle and Morcrette, 2006; Gabriel et al., 2007, 2011b; Gillet et al., 2009; Waugh et al., 2009; McCormack et al., 2011; Albers et al., 2013). However, possible effects of mesoscale ozone-gravity wave interaction in the upper stratosphere/lower mesosphere (USLM) have not been considered up to now.

The basic idea of the present paper can be summarized as follows. In the USLM, where the coupling between ozone photochemistry and temperature is particularly strong, the time-mean ozone mixing ratio $\mu_0(z)$ is decreasing with height ($\partial\mu_0/\partial z < 0$). Therefore, a local uplift of an air parcel initially forced by an upward propagating GW (with vertical velocity perturbation $w' > 0$) must lead to a local increase $\partial\mu'/\partial t > 0$ by both transport (because $-w'\partial\mu_0/\partial z' > 0$) and photochemistry (because the temperature-dependent ozone production increases in case of adiabatic cooling), and, hence, in the heating rate $Q'(\mu') > 0$, comparable to the latent heat release in the troposphere in case of condensation. Then, the induced perturbation $\Delta\theta' > 0$ (θ is potential temperature) reinforces the initial uplift, where the lapse rate $\partial(\theta_0 + \Delta\theta')/\partial z < \partial\theta_0/\partial z$ decreases



($\partial z = \text{constant}$) suggesting an effective *ozone adiabatic lapse rate* in the upper stratosphere analogously to the *moist adiabatic*
85 *lapse rate* in the troposphere. Overall, this process must lead to a significant local amplification of the initial GW amplitude
and, hence, to an over-exponentially growth of the amplitude during the upward level-by-level propagation through the
ULSM.

In Section 2, standard equations for GWs in a zonal mean background flow with and without linearized ozone-temperature
coupling are formulated to quantify the local amplitude amplification at a specific altitude and latitude. Then, in section 3,
90 the cumulative amplitude amplification during the propagation through the USLM is derived, based on an idealized approach
of the upward level-by-level propagation of GWs with specific horizontal and vertical wavelengths. Section 4 concludes
with summary and discussion.

2. Ozone-gravity wave interaction

95 In the following, ozone-gravity wave interaction is analysed based on standard equations describing GWs in a background
atmosphere, where the solutions are illustrated for southern summer conditions. The background is prescribed by monthly
and zonal mean temperature T_0 , ozone μ_0 and short-wave heating rate Q_0 of January 2001 (Figure 1, a-c) derived from a
simulation with the high-altitude general circulation and chemistry model HAMMONIA (details of the model are given by
Schmidt et al., 2010). The heating rate Q_0 (Figure 1c) is primarily due to the absorption of solar radiation by ozone and
100 largely agrees with southern summer solar heating rates derived from satellite measurements by Gille and Lyjak (1986) but
with somewhat smaller maximum values (in the order of $\sim 10\%$). Figure 1c shows that Q_0 is particularly strong in the upper
stratosphere and lower mesosphere (USLM) where $\partial\mu_0/\partial z < 0$ (the dashed line in Figure 1b indicates $\partial\mu_0/\partial z = 0$). The
HAMMONIA model includes 119 layers up to 250 km with increasing vertical resolution between ~ 0.7 km in the middle
stratosphere and ~ 1.4 km in the middle mesosphere, with a horizontal resolution of 3.75° ; in the following, this grid is used
105 to illustrate the analytic solutions of upward propagating GWs.

2.1 Local amplification of gravity wave amplitudes

Following Fritts and Alexander (2001), we consider standard equations (1)-(5) describing gravity wave propagation in a
background flow, with linear gravity wave perturbations T' , θ' , u' , v' , w' , p' and ρ' (T' is temperature, $\theta' = T'(p_0/p)^\kappa$ is
110 potential temperature, $p(z)$ is pressure, $p_0 = 1000$ hPa, z is altitude, u' , v' and w' are zonal, meridional and vertical wind
perturbations, p' and ρ' are the perturbations in pressure and density). Additionally, we include an ozone-dependent heating
rate perturbation $Q'(\mu')$ in the temperature equation (Eq. 5), and Eq. (6) for the ozone perturbation μ' with a temperature-
dependent perturbation in ozone photochemistry $S'(T')$, where $a(\varphi, z) > 0$ and $b(\varphi, z) > 0$ are linear coupling parameters as a
function of latitude φ and altitude z specified below ($\rho_0(z) = \rho_{00} \exp^{-(z-z_0)/2H}$ is background density, $H \sim 7$ km is scale height, ρ_{00}



115 is a reference value at altitude z_0 , u_0 is a zonal mean background wind, $d_0/dt = \partial/\partial t + u_0 \partial/\partial x$ where $\partial/\partial x$ and $\partial/\partial y$ denote the derivations in longitude and latitude, g is the gravity acceleration, f is the Coriolis parameter; the background shear terms $w' \partial u_0/\partial z$ and $w' \partial v_0/\partial z$ are neglected because of the Wentzel-Kramers-Brillouin or WKB approximation):

$$\frac{d_0 u'}{dt} + \frac{1}{\rho_0} \frac{\partial p'}{\partial x} = f v' \quad (1)$$

120

$$\frac{d_0 v'}{dt} + \frac{1}{\rho_0} \frac{\partial p'}{\partial y} = -f u' \quad (2)$$

$$\frac{d_0 w'}{dt} + \frac{1}{\rho_0} \frac{\partial p'}{\partial z} = g \frac{\theta'}{\theta_0} \quad (3)$$

$$125 \quad \frac{d_0 \rho'}{dt} + \frac{\partial u'}{\partial x} + \frac{\partial v'}{\partial y} + \frac{1}{\rho_0} \frac{\partial \rho_0 w'}{\partial z} = 0 \quad (4)$$

$$\frac{d_0 \theta'}{dt} + w' \frac{\partial \theta_0}{\partial z} = Q' \left(\frac{p_{00}}{p} \right)^{\kappa} = \frac{a}{\mu_0} \frac{d_0 \mu'}{dt} \quad (5)$$

$$\frac{d_0 \mu'}{dt} + w' \frac{\partial \mu_0}{\partial z} = S' = -b \mu_0 \frac{d_0 \theta'}{dt} \quad (6)$$

130

Setting $Q'=0$, the dispersion relation for gravity waves results from Eqs. (1)-(5) by introducing sinusoidal perturbations $X_1' = X_{a0} \cdot \exp[i(k_1 x + l_1 y + m_1 z - \omega_1 t)] \cdot \exp^{(z-z_0)/2H}$, where X_1' denotes the perturbation quantities, X_{a0} the initial amplitude at altitude z_0 at the lower boundary of the upper stratosphere, $\exp^{(z-z_0)/2H}$ the exponential growth of the amplitude due to decreasing density, k_1 and l_1 the horizontal and meridional wave number, $m_1 < 0$ the vertical wave number for upward propagating GWs with $|m_1| = 2\pi/L_{m1}$ and vertical wavelength L_{m1} , and ω_1 the frequency (here, the subscript 1 denotes the solutions for $Q'=0$). We focus on horizontal and vertical wavelengths $L_{h1} \geq 50$ km and $L_{m1} \leq 15$ km, where $k_{h1} = 2\pi/L_{h1}$ is the horizontal wave number given by $k_{h1} = (k_1^2 + l_1^2)^{1/2}$, therefore $(1 + k_{h1}^2/m_1^2) \approx 1$. Compressibility effects due to the vertical change in background density are excluded assuming $m_1^2 \gg 1/4H^2$, which is valid for vertical wavelengths $L_m \leq 30$ km. Then, the dispersion relation for the intrinsic frequency $\omega_{i1} = \omega_1 - k_1 u_0$ is given for the frequency range $N_0^2 > \omega_{i1}^2 > f^2$, where

140 $N_0^2 = (g/\theta_0) \cdot \partial \theta_0 / \partial z$ denotes the Brunt-Vaisala frequency:

$$\omega_{i1}^2 = \frac{N_0^2 k_{h1}^2 + m_1^2 f^2}{k_{h1}^2 + m_1^2} \approx N_0^2 \frac{k_{h1}^2}{m_1^2} + f^2 \quad (7)$$



For specifying the parameter b , we consider an initial perturbation of the vertical updraft $w'_1 > 0$, related to an adiabatic cooling term $d_0\theta'_1/dt = -w'_1 \cdot \partial\theta_0/\partial z < 0$, which leads to an initial ozone perturbation $\mu'_1 > 0$ due to the induced increase $d_0\mu'_1/dt = -w'_1 \cdot \partial\mu_0/\partial z > 0$ via transport, and to a change in ozone photochemistry described by $S'(T'_1)$. In the USLM region, ozone is very short lived and approximately in photochemical equilibrium (Brasseur and Solomon, 1995), i.e., for pure oxygen chemistry it is approximately given by

$$O_3 = \left(\frac{k_2}{k_3} M(O_2)^2 \frac{J_2(O_2)}{J_3(O_3)} \right)^{1/2} \quad (8)$$

where $J_2(O_2)$ and $J_3(O_3)$ are photo-dissociation rates, and $k_2 = 6.0 \cdot 10^{-34} \cdot (300/T)^{2.3} \text{ cm}^6\text{s}^{-1}$ and $k_3 = 8.0 \cdot 10^{-12} \cdot \exp(-2060/T) \text{ cm}^3\text{s}^{-1}$ chemical reaction rates for ozone production, $O + O_2 + M \rightarrow O_3 + M$, and ozone loss, $O + O_3 \rightarrow 2O_2$ (Appendix C of Brasseur and Solomon, 1995; Table 2 of Schmidt et al., 2010). Accordingly, following Brasseur and Solomon (1995), a relative change in ozone $\Delta\mu_T/\mu_0 = \Delta O_3/O_3$ due to a change in temperature ΔT is given by

$$\frac{\Delta\mu_T}{\mu_0} = \frac{1}{2} \frac{\Delta(k_2/k_3)}{(k_2/k_3)} = -\frac{1}{2} \left(\frac{2.3}{T_0} + \frac{2060}{T_0^2} \right) \Delta T \equiv -b_0(T_0) \Delta T \quad (9)$$

Then, defining $b = b_0 \cdot (p/p_{00})^\kappa$ and introducing a total temperature change $\Delta T/\Delta t$ within a background flow described by $d_0T'/dt = (p/p_{00})^\kappa \cdot d_0\theta'/dt$, the change S' is given by

$$S' = \frac{\Delta\mu_T}{\Delta t} = \frac{\Delta\mu_T}{\Delta T} \frac{\Delta T}{\Delta t} = -\mu_0 b \frac{d_0\theta'}{dt} \quad (10)$$

which is the right-hand term of Eq. (6). Overall, the initial updraft w'_1 leads to a local increase in ozone via transport, and the related adiabatic cooling to an increase in ozone because of the induced change $S' > 0$. The height-dependence of b is specified by considering that the ozone photochemistry of the USLM region is related to the spatial structure of Q_0 , which is characterized by a Gaussian-type height-dependence centered at the maximum of Q_0 and rapid decrease with latitude in the extra-tropical winter hemisphere (see Figure 1c). Therefore, b is multiplied with the normalized factor $hz = Q_0/Q_{00}$, where Q_{00} is the averaged profile of Q_0 over the summer hemisphere ($b \rightarrow b \cdot hz$, where $hz(z) \approx 1$ in the summer upper stratosphere at the altitude where Q_0 reach maximum values). A similar approach of Gaussian-type height-dependence in ozone-temperature coupling was successfully used by Gabriel et al. (2011a) to analyze observed planetary-scale waves in the ozone distribution. Following previous works (e.g., Cordero and Nathan, 1998, 2000; Nathan et al., 2007; Ward et al., 2010; Gabriel et al., 2011a), the sensitivity of the upper stratospheric heating rate to a change in ozone is approximately described by the linear



175 approach $\Delta Q_{\mu} \approx A \cdot \Delta \mu$, where $A = A(\varphi, z)$ is a time-independent linear function. If we assume the same sensitivity for both the slowly varying background and the mesoscale GW perturbation propagating within the background flow, $Q_0 \approx A \cdot \mu_0$ and $Q' \approx A \cdot \mu'$, we may write $\Delta Q_{\mu} / \Delta \mu = Q_0 / \mu_0 = Q' / \mu'$. At a specific altitude z or pressure level $p(z)$, we consider a GW perturbation over the vertical scale of a vertical wavelength, $\Delta z = L_m$. Then, considering that $\partial \mu' / \partial z = i m \mu' = (\tau_i / L_m) \cdot (-i \omega_i \mu')$ with $\tau_i = 2\pi / \omega_i$, the first-order heating rate perturbation is given by

$$180 \quad Q' = L_m \frac{\partial Q'}{\partial z} \approx L_m \frac{\Delta Q_{\mu}}{\Delta \mu} \frac{\partial \mu'}{\partial z} = \tau_i \frac{Q_0}{\mu_0} \frac{d_0 \mu'}{dt} \quad (11)$$

185 which is the right-hand side of Eq. (5) when defining $a_0 = \tau_i Q_0$ and $a = a_0 \cdot (p_0 / p)^{\kappa}$. Except in polar summer regions, the effect of Q' is limited by the length of daylight (here denoted by τ_{day}) in case of large wave periods; therefore, we set the time increment to $\tau_i = \tau_{\text{day}}$ in case of $\tau_i > \tau_{\text{day}}$, which reduces the effect of Q' during the time period of 24 hours (e.g., $\tau_i \leq 12$ hours over the equator). Overall, assuming again an initial updraft $w'_i > 0$, the induced local increase in ozone $\mu' > 0$ at a pressure level $p(z)$ leads to a heating rate perturbation $Q' > 0$ at this level counteracting to the initial adiabatic cooling and therefore reinforcing the initial updraft.

Note here that the use of $\Delta z = L_m$ in Eq. (11) provides a suitable measure of the local effect of ozone-temperature coupling on the GW amplitudes over the vertical distance L_m . It is also possible to set a smaller vertical scale $\Delta z < L_m$ leading to smaller values $Q'_{\Delta z} = (\Delta z / L_m) \cdot Q'$ at a specific level, where Δz denotes, for example, the distances of a vertical grid used in a numerical model; this modification does not change the local effect over the vertical distance L_m but it provides better vertical resolution when calculating the cumulative amplitude amplification during the upward level-by-level propagation particularly in case of small vertical wavelengths or small vertical group velocities as described in the next subsection.

195 The parameterizations of Q' and S' provide a useful modification of the temperature tendency when introducing $d_0 \mu' / dt$ of Eq. (6) into (Eq. 5):

$$(1+ab) \frac{d_0 \theta'}{dt} + w' \left(\frac{\partial \theta_0}{\partial z} + \frac{a}{\mu_0} \frac{\partial \mu_0}{\partial z} \right) = 0 \quad (12)$$

200 Here, the amplification factor $1+ab$ (with $ab > 0$) describes the feedback of the GW-induced ozone perturbation to the change in temperature, and $\partial \theta_0 / \partial z + (a / \mu_0) \cdot \partial \mu_0 / \partial z$ an *ozone adiabatic lapse rate* which is – in the USLM region – smaller than $\partial \theta_0 / \partial z$ because of $\partial \mu_0 / \partial z < 0$. Alternatively, we may write:

$$\frac{d_0}{dt} \left(\frac{g}{\theta_0} \theta' \right) + N_{\mu}^2 w' = 0 \quad (13)$$



205 with

$$N_{\mu}^2 = \frac{N_0^2 + N_c^2}{(1+ab)} \quad (14)$$

where $N_c^2 = (g/\theta_0) \cdot (a/\mu_0) \cdot \partial\mu_0/\partial z$. Like for the lapse rate, N_{μ}^2 is smaller than N_0^2 because $N_c^2 < 0$ and $(1+ab) > 1$. If ozone-
 210 temperature coupling becomes weak, below and above the USLM region, N_{μ}^2 converges to N_0^2 .

Analogously to the standard solution given above, we introduce sinusoidal GW perturbations of the form
 $X_2' = X_{\mu 0} \cdot \exp[i(k_2x + l_2y + m_2z - \omega_2t)] \cdot \exp^{(z-z_0)/2H}$ in Eqs. (1)-(4) and (13) (here, the subscript 2 denotes the solutions with ozone-
 gravity wave coupling) which leads to the modified dispersion relation

$$215 \quad \omega_{i2}^2 = \frac{N_{\mu}^2 k_{h2}^2 + m_2^2 f^2}{k_{h2}^2 + m_2^2} \approx N_{\mu}^2 \frac{k_{h2}^2}{m_2^2} + f^2 \quad (15)$$

where $\omega_{i2} = \omega_2 - k_2 u_0$ and $k_{h2} = (k_2^2 + l_2^2)^{1/2}$.

Eq. (13) provides an evident measure of the local amplification of a GW amplitude at a specific altitude z or pressure level
 $p(z)$. On the one hand, introducing the same initial adiabatic cooling $d\theta'_1/dt$ either with or without ozone-temperature
 220 coupling leads to an increase in the updraft described by $w_2' = w_1' \cdot (N_0^2/N_{\mu}^2)$. Consistently, introducing the same initial updraft
 $w_1' N_0^2$ leads to $d\theta'_2/dt = d\theta'_1/dt$ or $-i\omega_{i2}\theta_2' = -i\omega_{i1}\theta_1'$. Then, combining $-i\omega_{i2}\theta_2' = -N_{\mu}^2 w_2'$ and $-i\omega_{i1}\theta_1' = -N_0^2 w_1'$ suggests that
 the amplitude $\theta_{\mu} = \theta_{\mu 0} \cdot \exp^{(z-z_0)/2H}$ is stronger than $\theta_a = \theta_{a0} \cdot \exp^{(z-z_0)/2H}$ by the factor $\omega_{i1}/\omega_{i2} = N_0^2/N_{\mu}^2 \geq 1$:

$$\theta_{\mu} = \theta_a \cdot (\omega_{i1}/\omega_{i2}) \quad (16)$$

225

Overall, the introduced process of ozone-temperature coupling leads to decrease in the GW frequency and a corresponding
 amplification in the GW amplitude described by the factor ω_{i1}/ω_{i2} or N_0^2/N_{μ}^2 . Note that vertical variations in N_0^2 could affect
 the increase in amplitude with height particularly in the summer upper mesosphere; therefore, N_0^2 is vertically averaged over
 the USLM region (from 30 hPa to 0.03 hPa, or ~25 km to ~70 km altitude) to focus on the effects of ozone-gravity wave
 230 interaction only. Note also that the relation $\omega_{i1}/\omega_{i2} = N_0^2/N_{\mu}^2$ implies not only a change in amplitude but also a slight change in
 the relation of horizontal and vertical wavenumber described by $(k_{h2}/m_2) = (N_{\mu}^2/N_0^2)(k_{h1}/m_1) + f^2(N_{\mu}^2 - N_0^2)/(N_0^2 \cdot N_{\mu}^2)$, i.e., a
 slight change in the direction of upward propagating GWs which is perpendicular to the angle α of the phase lines defined by
 $\cos(\alpha) = \pm(k_h/m)$. However, as illustrated in the following, ozone-gravity wave interaction is particularly relevant for a range
 of wavelengths and periods where the induced changes in α are very small (for $L_{m1}/L_{kh1} < 0.05$, or wave periods $\tau_i > 2h$, the
 235 change in α is less than $1 \cdot 10^{-4}$ degree).



Figure 1d-f shows the factor $1+ab$ and the quotient N_0^2/N_μ^2 for a GW with horizontal and vertical wavelengths $L_k=500$ km and $L_m=5$ km, and the quotient N_0^2/N_μ^2 for a GW with $L_k=800$ km and $L_m=3$ km, which are typical representatives of mesoscale GWs forced by cyclones or fronts, or by the orography of the Southern Andes. In the first example, the factor $1+ab$ (Figure 1d) contributes to the local amplification of the GW amplitude by up to 6-8%, and the overall factor $N_0^2/N_\mu^2=(1+ab)\cdot N_0^2/(N_0^2+N_c^2)$ (Figure 1e) by up to 8-12% (including a decrease in the lapse rate of up to 3% described by $(N_0^2+N_c^2)/N_0^2$, here not shown). The second example (Figure 1f) shows that the factor N_0^2/N_μ^2 is larger in case of larger horizontal and smaller vertical wavelength, reaching local amplifications of up to 12% to 14% (shaded areas denote the latitudinal range where the amplification is reduced due to the length of daylight, i.e., where $\tau_i > \tau_{\text{day}}$).

For illustration of the induced local change in ozone (Figure 2 a-d), we assume an initial GW perturbation θ'_1 with exponentially growing amplitude $\theta_a=\theta_{a0}\cdot\exp^{(z-z_0)/2H}$, with an initial temperature amplitude T_a of 1 K at $z_0\approx 35$ km ($p=6.28$ hPa) increasing to ~ 8 K at $z\approx 65$ km ($p=0.1$ hPa). Introducing the associated perturbation $w'_1=-\frac{\partial\theta_0}{\partial z}\cdot d_0\theta'_1/dt$ in Eq. (6) leads to $d_0\mu'_1/dt=[\frac{\partial\mu_0}{\partial z}/(\frac{\partial\theta_0}{\partial z})-b\mu_0]\cdot d_0\theta'_1/dt$, and, considering $d_0\mu'_1/dt=-i\omega_{i1}\mu'_1$ and $d_0\theta'_1/dt=-i\omega_{i1}\theta'_1$, to an initial ozone perturbation $\mu'_1=\theta'_1\cdot[\frac{\partial\mu_0}{\partial z}/(\frac{\partial\theta_0}{\partial z})-b\mu_0]$, where $\theta'_1<0$ and $\mu'_1>0$ in case of $w'_1>0$. For $L_k=500$ km and $L_m=5$ km, the contributions $\mu'(\text{TR})=\theta'_1\cdot[\frac{\partial\mu_0}{\partial z}/(\frac{\partial\theta_0}{\partial z})]$ related to transport (Figure 2a) and $\mu'(\text{CH})=-b\mu_0\theta'_1$ related to S' (Figure 2b) sum up to a total change of $\mu'\approx 0.2$ to 0.5 ppm (Figure 2c) or $\mu'/\mu_0\approx 5$ to 10 % (Figure 2d) in the USLM region where the feedback to the heating rate is particularly strong.

The related local change in the heating rate (Figure 2e) is given by comparing Eq. (5) with and without ozone-temperature coupling. Assuming the same initial updraft or adiabatic cooling as above leads to $(w'_2-w'_1)(\frac{\partial\theta_0}{\partial z})=Q'(\mu'_1)$, or, when introducing $w'_2=(\omega_{i1}/\omega_{i2})\cdot w'_1$, to $Q'(\mu'_1)=(\omega_{i1}/\omega_{i2}-1)(-i\omega_{i1}\theta'_1)=a\omega_{i1}\mu'_1\mu_0^{-1}$ (where $Q'(\mu'_1)>0$ in case of $w'_1>0$). Figure 2e shows that $Q'(\mu'_1)$ reach values of 0.15 K hr⁻¹ over the tropics and 0.25 K hr⁻¹ at southern summer polar latitudes. Then, consistently with Eq. (16), we yield $\theta'_2-\theta'_1=(\omega_{i1}/\omega_{i2}-1)\cdot\theta'_1$ with $(\omega_{i1}/\omega_{i2}-1)=-a\mu_0^{-1}[\frac{\partial\mu_0}{\partial z}/(\frac{\partial\theta_0}{\partial z})-b\mu_0]$ for the change in the temperature perturbation, with values of 0.2 K to 0.3 K in the USLM region (Figure 2f).

For other initial wavelengths (or associated frequencies), the latitude-height dependence is very similar to those shown in Figure 1 (d-f) and Figure 2, whereas the magnitude of the amplification factor ω_{i1}/ω_{i2} becomes smaller in case of increasing vertical and decreasing horizontal wavelengths, or decreasing frequencies, as illustrated in Figure 3 for an altitude where ω_{i1}/ω_{i2} reach maximum values (1.156 hPa or ≈ 47 km altitude). Figure 3a shows values of $\omega_{i1}/\omega_{i2}>1.02$ for wave periods of $\tau_i>2$ h steadily increasing with increasing initial period up to values between 1.14 and 1.15. This value is limited, on the one side, because of the increasing duration of nighttime with latitude towards equatorial and northern winter regions (denoted by shaded areas), and, on the other side, because of the increasing Coriolis force in southern summer mid- and polar regions (i.e., because of $\omega_{i1}^2>f^2$).

Consistently, the amplification factor is increasing with decreasing vertical but increasing horizontal wavelength (Figures 3b and 3c show examples for 70°S and 30°S), where the values are limited by the length of daylight in case of small relations



L_m/L_k denoting the conditions where $\tau_i > \tau_{\text{day}}$ (Figure 3c, shaded area). Figure 3 also indicates that the examples with $L_k=500$ km and $L_m=5$ km (Figures 1e) and $L_k=800$ km and $L_m=3$ km (Figure 1f) represent scales where ozone-gravity wave interaction is particularly efficient.

Overall, Figures 1 (d-f), 2 and 3 illustrate the local amplification of GW amplitudes at a specific level and a specific time; as far as the GWs are continuously propagating upward through several levels where $\omega_{i1}/\omega_{i2}-1 > 0$, the amplification will be successively reinforced at each level. This cumulative amplification can lead to an efficient over-exponential growth of the GW amplitudes as demonstrated in the next subsection.

275

2.2 Upward propagating GWs in a background flow

In the following, a solution of the cumulative amplification during the vertical level-by-level propagation is derived, excluding – to a first guess – other effects like small-scale diffusion or wave breaking processes. Following Huygens principle, each point of a propagating wave front at a specific level is the source of a new wave at this level, i.e., a single upward propagating GW, which is amplified at a level z_{j-1} , is the initial perturbation amplified at the next level z_j . For illustration (Figure 4, a-c), we choose an initial GW with horizontal and vertical wavelengths $L_m=500$ km and $L_m=5$ km as above, where the vertical distance between the levels z_{j-1} and z_j is set by the initial vertical wavelength $\Delta z=L_m$. First, we focus on polar latitudes during southern polar summer (70°S) with daylight conditions only, then we consider the modification for mid- and equatorial latitudes where GWs with weak vertical group velocities propagate through the USLM during both daylight and nighttime.

For orientation, Figure 4a shows the profiles ω_{i1}/ω_{i2} for $L_k=500$ km and $L_m=5$ km at 70°S (solid), and, for comparison, for $L_m=3$ km (dashed) and $L_m=9$ km (dotted), indicating the altitude range where ozone-temperature coupling is relevant (note that the depicted distance of pressure levels represents approximately a 5 km distance in altitude). Beginning with a first level at $z_s \approx 35$ km (6.28 hPa), the wave propagates through 8 layers between ≈ 35 km and ≈ 70 km (0.06 hPa) where the amplification of the amplitude is relevant. At each of these levels, denoted by $z_j = z_s + (j-1) \cdot \Delta z$ ($j=1, n$; here $n=8$), the amplitude will be amplified by the local factor $\omega_{i1}(z_j)/\omega_{i2}(z_j)$. Starting with an exponentially growing amplitude $T_a(z) = T_a(z_s) \cdot \exp^{(z-z_s)/2H}$ (where we set again $T_a(z_s)=1$ K), we yield a new amplitude $T_{a1}(z_1) = T_a(z_1) \cdot \omega_{i1}(z_1)/\omega_{i2}(z_1)$ at the level z_1 defining a new exponentially growing amplitude $T_{\mu 1}(z) = T_{a1}(z_1) \cdot \exp^{(z-z_1)/2H}$. Then, we yield $T_{a2}(z_2) = T_{\mu 1}(z_2) \cdot \omega_{i1}(z_2)/\omega_{i2}(z_2)$ at the level z_2 defining $T_{\mu 2}(z) = T_{a2}(z_2) \cdot \exp^{(z-z_2)/2H}$, and so on. Finally, the amplitude at the level z_n in the middle mesosphere is described by

295

$$T_{\mu n}(z) = T_a(z) \cdot \prod_{j=1}^n \left[\frac{\omega_{i1}(z_j)}{\omega_{i2}(z_j)} \right], \quad (17)$$



where the product symbol $\prod_{j=1, n}$ denotes the multiplication with $\omega_{i1}(z_j)/\omega_{i2}(z_j)$ at each level $z_1 \leq z_j \leq z_n$.

300 Figure 4b shows the initial amplitude T_a (blue line) and the series of the successively amplified amplitudes $T_{\mu 1}, T_{\mu 2}, \dots, T_{\mu n}$ (from light blue towards red line), and Figure 4c the related series of constant relative values $T_{\mu 1}/T_a, T_{\mu 2}/T_a, \dots, T_{\mu n}/T_a$ starting at the level z_j (solid lines) together with the previous values starting at z_{j-1} multiplied by the factor ω_{i1}/ω_{i2} (dotted lines), illustrating the successive over-exponential growth of the amplitude during the upward level-by-level propagation. Finally, the amplitudes converge to $T_{\mu n}(z)$ when reaching the upper mesosphere, where $T_{\mu n}(z)$ is stronger than $T_a(z)$ by a
 305 factor of ~ 1.47 . Figure 4c also shows the fitted relative increase of the amplitude T_{μ}/T_a (thick red line) describing the continuous over-exponential growth of the amplitude, where $T_{\mu}(z)$ is defined by

$$T_{\mu}(z) = h_s(z) \cdot T_a(z) + h_m(z) \cdot T_{\mu n}(z) \quad (18)$$

310 with weighting functions $h_s = p_0^{1.5}/(p_0^{1.5} + p_m^{1.5})$ and $h_m = 1 - h_s$, where p_0 is the background pressure and $p_m(70^\circ\text{S}) \approx 0.96$ hPa the level of the maximum of ω_{i1}/ω_{i2} (note that the height of this maximum is slightly decreasing from $p_m \approx 0.89$ hPa over the south pole to $p_m \approx 1.3$ hPa over the equator).

In the following, the fitted profiles T_{μ} are used for further examinations with different horizontal and vertical wavelengths, where the vertical level-by-level amplification is calculated by using the distances $\Delta z = \Delta z_H$ of the vertical grid of
 315 HAMMONIA instead of $\Delta z = L_m$. This includes a smaller amplification factor $F_{\omega} = \omega_{i1}/\omega_{i2}$ over the vertical distance Δz_H because of the smaller heating rate perturbation $Q'_{\Delta z_H} = (\Delta z_H/L_m) \cdot Q'$ (see Eq. (11 and related discussion); however, the resulting difference in the local amplification over the vertical distance L_m are nearly the same except some small differences of less than 0.5% due to the different vertical resolution (i.e., $F_{\omega}(\Delta z = L_m) \approx 1 + (F_{\omega}(\Delta z = \Delta z_H) - 1) \cdot (L_m/\Delta z_H)$). Also the resulting cumulative amplification in the upper mesosphere remains nearly unchanged ($T_{\mu n}(\Delta z = L_m) \approx T_{\mu n}(\Delta z = \Delta z_H)$, where n_h is the
 320 number of the HAMMONIA levels in the USLM), where small differences between $T_{\mu n_h}$ and $T_{\mu n}$ of less than 10 % occur only at mid- and equatorial latitudes in case of small vertical wavelengths (or small vertical group velocities) when considering the vertical propagation during both daylight and nighttime described below.

Figure 4e illustrates the dependence of the amplitude amplification on the horizontal and vertical wavelengths L_k and L_m at 70°S , where it is not affected by nighttime conditions. In comparison to the example of $L_k = 500$ km and $L_m = 5$ km leading to
 325 a cumulative amplification of ~ 1.47 (red, solid line), a larger vertical wavelength of $L_m = 9$ km leads to a smaller value of ~ 1.15 (red, dotted line), but a smaller vertical wavelength of $L_m = 3$ km to a larger value of ~ 2.27 (red, dashed line), because the induced increase in the ozone perturbation μ' produces a heating rate perturbation Q' within a shorter (in case of $L_m = 9$ km) or larger (in case of $L_m = 3$ km) time increment τ_i . For the same reason, the amplification is generally larger if the horizontal wavelength L_k is larger, e.g., in case of $L_k = 800$ km, the final amplification in the upper mesospheric amplitudes



330 amounts to ~ 1.22 for $L_m=9$ km (purple, dotted line), ~ 1.63 for $L_m=5$ km (purple, solid line), and ~ 2.56 for $L_m=3$ km (purple, dashed line).

The related gravity wave potential energy density (GWPED, here denoted by E) is derived following Kaifler et al. (2015):

$$E = \frac{1}{2} \left(\frac{g}{N} \right)^2 \left(\frac{T'}{T_0} \right)^2 \quad (19)$$

335

Introducing $T'=T_2'$ and $N=N_\mu$, or $T'=T_1'$ and $N=N_0$, leads to the case with (E_μ) or without (E_a) ozone-gravity wave interaction. Figure 4f shows the relative amplitudes E_μ/E_a related to Figure 4e. In case of $L_k=500$ km (red lines), the final amplification reach values of ~ 1.32 for $L_m=9$ km (dotted), ~ 2.17 for $L_m=5$ km (solid), and ~ 5.21 for $L_m=3$ km (dashed), and in case of $L_k=800$ km (purple) values of ~ 1.50 for $L_m=9$ km (dotted), ~ 2.70 for $L_m=5$ km (solid), and ~ 6.62 for $L_m=3$ km (dashed). Overall, these factors provide a first-order estimate of the effect of ozone-gravity wave coupling at 70°S during polar summer, i.e., in case of large horizontal (≥ 500 km) and small vertical (≤ 5 km) wavelengths, we find cumulative amplifications in the upper mesosphere in the order of ~ 1.5 to ~ 2.5 in the temperature perturbations and in the order of ~ 3 to ~ 7 in the related GWPED.

340

For mid- and equatorial latitudes, daylight-nighttime conditions are considered by setting the amplification factor to $F_d=\omega_{i1}/\omega_{i2}$ during daylight but to $F_d=1$ during nighttime over the vertical wave propagation distance of one full day. In detail, we define the parameter $L_{\text{day}}=(\tau_{\text{day}}-0.5\cdot\tau_0)/(0.5\cdot\tau_0)$, where $\tau_0=24$ hours and τ_{day} is the duration of daylight within 24 hours at the latitude φ (with $L_{\text{day}}=1$ during polar summer and $L_{\text{day}}=0$ at the equator). Further, considering the vertical group velocity $c_{gz}=\partial\omega_{i1}/\partial m_1=-(\omega_{i1}^2-f^2)/\omega_{i1}^2$ (with initial frequency ω_{i1} and vertical wavelength m_1 as first guess), the sinusoidal wave propagation structure between the middle stratosphere and middle mesosphere is described by $L_{cgz}=\cos(2\pi\tau_0\cdot(z-z_m)/c_{gz})$ changing periodically between 1 and -1 over one wavelength, where z and z_m are given in km and c_{gz} in km hr^{-1} , and where $L_{cgi}=1$ at the level p_m or altitude $z_m(p_m)$. Then, the combined parameter $L_d=L_{\text{day}}+L_{cgi}$ separates the vertical propagation distance into daylight and nighttime fractions by defining a constant value $C_d=1$ in case of $L_d>1$ and $C_d=0$ in case of $L_d\leq 1$, where the factor $F_d=1+C_d\cdot((\omega_{i1}/\omega_{i2})-1)$ provides $F_d=\omega_{i1}/\omega_{i2}$ in case of daylight and $F_d=1$ in case of nighttime.

345

As an example, Figure 4d shows the profile of the resulting amplification factor F_d at 10°S for a GW with $L_k=500$ km and $L_m=5$ as above, with an associated vertical group velocity c_{gz} of about 7 km per 12 hours, illustrating that we define $F_d(z_j)=\omega_{i1}(z_j)/\omega_{i2}(z_j)$ where z_j is located in the daylight region (red) but $F_d(z_j)=1$ where z_j is located in the nighttime region (blue). The indicated vertical wave propagation distance during daylight increases towards southern summer polar latitudes but decreases towards northern winter polar latitudes. Note here that, for vertical wavelengths examined in the present paper ($L_m\leq 15$ km), a vertical shift of the phase – as defined by the altitude z_m in the definition of L_{cgz} – does not have a significant impact on the cumulative amplification of the GW amplitudes because of the Gaussian-type structure of the profile of $F_d=\omega_{i1}/\omega_{i2}$, which has been verified by several test calculations with other altitudes than z_m .

350



For the same example, Figure 5 illustrates the latitudinal dependence of the cumulative amplification of the temperature perturbation (indicated by T_{μ}/T_a , Figure 5a) and the related GWPED (indicated by E_{μ}/E_a , Figure 5b). The values decrease from $T_{\mu}/T_a \approx 1.5$ and $E_{\mu}/E_a \approx 2.4$ over southern summer polar latitudes towards $T_{\mu}/T_a \approx 1.2$ and $E_{\mu}/E_a \approx 1.4$ at lower mid-latitudes
365 (40°S), and then less rapidly towards values of $T_{\mu}/T_a \approx 1.1$ and $E_{\mu}/E_a \approx 1.2$ at 20°N. Overall, although the amplification of the GW amplitudes decrease rapidly with the decrease in the length of daylight, it is still quite strong at mid-latitudes.

Figure 6 shows the relations T_{μ}/T_a (Figure 6a) and E_{μ}/E_a (Figure 6b) at upper mesospheric levels (0.01 hPa, ~80 km) for different horizontal and vertical wavelengths as used for Figures 4e and 4f. For both $L_k=500$ km (red) and $L_k=800$ km (purple), the amplifications of the temperature perturbations and of the related GWPED are strongest for $L_m=3$ km (dashed
370 lines), at polar latitudes with values between 2.5 to 3 in T_{μ}/T_a and 7 to 9 in E_{μ}/E_a , and at mid- and equatorial latitudes between 1.5 to 1.8 in T_{μ}/T_a and 2.4 to 3.5 in E_{μ}/E_a . These values decrease with increasing vertical wavelength, i.e., when changing to $L_m=5$ km (solid lines) or $L_m=9$ km (dotted lines) roughly to ~1.7 or ~1.25 in T_{μ}/T_a and ~3.0 or ~1.5 in E_{μ}/E_a at polar latitudes, and roughly to ~1.25 or ~1.2 in T_{μ}/T_a and ~1.5 or ~1.25 in E_{μ}/E_a at mid- and equatorial latitudes. Overall, the examples of the small vertical and large horizontal wavelengths are quantitatively in agreement with the over-exponential
375 growth of GW amplitudes observed by Kaifler et al. (2015) and Baumgarten et al. (2017).

Note here that the vertical momentum flux terms $F_{GW}=\rho_0(u'w')$ can be derived from local profiles T' if the background is known, i.e. by $F_{GW}=\rho_0 E \cdot (k/m)$ (Ern et al., 2004). Therefore, the amplification of the GW amplitudes must lead to the same amplification of the flux term F_{GW} and, if the GWs do not break at lower levels, of the associated gravity wave drag $GWD=-\rho_0^{-1} \partial F_{GW} / \partial z$ in the upper mesosphere, suggesting an important effect of ozone-gravity wave interaction on the
380 meridional mass circulation particularly at polar latitudes. However, more detailed investigations need extensive numerical model simulations with a spectrum of resolved GWs which is beyond the scope of the present paper.

Note also that the decrease in the frequency towards $\omega_{i2} < \omega_{i1}$ includes a slight decrease in the vertical group velocity towards $c_{gz2} < c_{gz1}$, which can additionally strengthen the process of amplitude amplification because the wave propagates somewhat more slowly through the ULSM region. However, this effect is at least one order smaller than the first-order process
385 described above as derived from test calculations including this effect. For example, for $L_k=500$ km and $L_m=5$ km, c_{gz2} is smaller than c_{gz1} by 15% to 20% at southern summer polar latitudes and 5% to 10% at mid- and equatorial latitudes. Subsequently, the local amplification factor $F_d(c_{gz2})$ is stronger than $F_d(c_{gz1})$ by 2% to 3% at polar latitudes and less than 1% at mid- and equatorial latitudes. Including this change into the successive level-by-level propagation leads to a weak successive increase in the cumulative amplifications by ~5% at 1 hPa to ~10% at 0.01 hPa at polar summer latitudes, and by
390 only ~1% at 1 hPa to ~2% at 0.01 hPa at mid- and equatorial latitudes.

We also estimate the sensitivity of the amplitude amplification on the ozone background μ_0 , considering the observed long-term changes in upper stratospheric ozone in the order of up to -8% per decade (e.g., Sofieva et al., 2017; WMO, 2018), and the uncertainty in the maximum of the heating rate Q_0 which is smaller in the used HAMMONIA data in the order of ~10% compared to those derived from satellite measurements, as mentioned above. In case of a 10%-reduction in ozone, the



395 cumulative amplification in the upper mesospheric GW amplitudes is weaker by about 5% for the example with $L_m=5$ km
and 10% for $L_m=3$ km (i.e., at 70°S , we yield a cumulative amplification of ~ 1.4 to ~ 2.25 instead of ~ 1.5 to ~ 2.5), and the
related amplification of the GWPED is weaker by about 10% for $L_m=5$ km and 20% for $L_m=3$ km (at 70°S , a cumulative
amplification of ~ 2.7 to ~ 7.2 instead of ~ 3 to ~ 9). Analogously, in case of an increase in Q_0 by 10%, the cumulative
amplification is stronger by 5% or 10% in the GW amplitudes and by 10% or 20% in the related GWPED amplitudes.

400

3 Summary and conclusions

The present paper shows that ozone-gravity wave interaction in the upper stratosphere/lower mesosphere (USLM) leads to a
stronger increase of gravity wave (GW) amplitudes with height during daylight than nighttime, particularly during polar
summer. The results include information on both the local amplification of the GW amplitudes and the cumulative increase
405 of the amplitudes during the upward propagation of the wave from middle stratosphere to upper mesosphere.

In a first step, standard equations describing upward propagating GWs with and without linearized ozone-gravity wave
coupling are formulated, where an initial sinusoidal GW perturbation in the vertical ozone transport and temperature-
dependent ozone photochemistry produces a heating rate perturbation as a function of the initial intrinsic frequency, which
determines the local duration of the perturbation over the distance of the initial vertical wavelength. The solution reveals a
410 decrease of the intrinsic frequency due to ozone-gravity wave coupling due to both the decreasing lapse rate (or Brunt-
Vaisala frequency) and the positive feedback of the coupling on the initial GW perturbation, and an associated local increase
of the GW amplitude by a factor $\omega_1/\omega_2 \geq 1$ defined by the relation of the intrinsic frequencies without (ω_1) and with (ω_2)
ozone-gravity wave coupling. This amplitude amplification is dependent on the horizontal and vertical wavelengths, L_k and
 L_m , where the effect is most efficient for GWs with $L_k \geq 500$ km and $L_m \leq 5$ km, or initial frequencies $\tau_i \geq 4$ hours, representing
415 GWs forced by cyclones or fronts, or by the orography of mountain ridges like the Southern Andes. For southern summer
conditions, strongest local amplitude amplifications of about 5% to 15% over the perturbation distance of one vertical
wavelength are located near the stratopause, with peak values over the equator and over summer polar latitudes.

In a second step, an analytic approach of the upward level-by-level propagation of the GW perturbations with and without
ozone-gravity wave interaction reveals the cumulative amplitude amplification, where the wave is propagating upward with
420 the vertical group velocity defined by the initial GW parameters, and where daylight-nighttime conditions at mid- and
equatorial regions are considered. Representative examples with different initial wavelengths illustrate that the continuous,
over-exponential increase of both the GW amplitudes and the related gravity wave potential energy density (GWPED)
converge to much stronger amplitudes in the upper mesosphere during daylight than nighttime. This effect is strongly
decreasing with latitude between summer polar and mid-latitudes because of the decrease in the length of daylight, nearly
425 constant at equatorial latitudes, and decreasing again with latitude towards insignificant values in the winter extra-tropics.
For GWs with horizontal wavelengths between $L_k=500$ km and $L_k=800$ km, and a vertical wavelength of $L_m=3$ km, the



amplitudes of the GWPED in the upper mesosphere are stronger during daylight than nighttime by a factor ~ 2.5 to ~ 3.5 at mid-latitudes, and by a factor ~ 7 to ~ 9 at polar latitudes, which are quantitatively in agreement with the observations of Baumgarten et al. (2017) and Kaifler et al. (2015).

430 The variety of horizontal and vertical wavelengths used in the present paper are representative for mesoscale GWs in the USLM region. Observations suggest characteristic vertical wavelengths of GWs between ~ 2 - 5 km in the lower stratosphere increasing to ~ 10 - 30 km in the upper mesosphere, but also the existence of large vertical wavelengths greater than 10 km in the stratosphere particularly above convection in equatorial regions (e.g., Alexander, 1998; McLandress et al., 2000; Fritts and Alexander, 2003; Hocke et al., 2016; Baumgarten et al., 2018). The results of the present paper suggests that the effect

435 of ozone-gravity wave coupling decreases with increasing vertical wavelengths $L_m \geq 9$ km but strongly increases with decreasing vertical wavelengths $L_m \leq 5$ km. The latter could be responsible for the more pronounced gravity wave breaking and dissipation processes in the upper stratosphere during daylight than nighttime, and – subsequently – for the more prominent GWs with larger vertical wavelengths of $L_m \geq 5$ km in the measurement profiles, as observed by Baumgarten et al. (2018) during a 10-day measurement campaign in May 2016.

440 Current state-of-the-art general circulation models (GCMs) usually use a variety of prescribed tropospheric sources and tuning parameters in the parameterized gravity wave drag (GWD) parameterizations forcing the middle atmospheric circulation (e.g., McLandress et al., 1998; Fritts and Alexander, 2003; Garcia et al., 2017), where the extreme low temperatures observed in the summer upper mesosphere provide an important benchmark for the quality of the upwelling branch and the associated adiabatic cooling produced by the models. Including ozone-gravity wave interaction into the

445 GCMs might lead to a substantial improvement of the used GWDs and the associated processes driving the summer mesospheric circulation, because the related over-exponential increase in the GWPED must lead to a similar increase in the vertical momentum flux term determining the GWD. However, the incorporation of ozone-gravity wave interaction in a state-of-the-art GCM using a GWD, or in a numerical model with resolved GWs, needs extensive test simulations, which is beyond the scope of the present paper.

450 Current GCMs particularly indicate significant changes in the time-mean circulation of the upper mesosphere due to the stratospheric ozone loss over Antarctica during southern spring and early summer via the induced changes in the GWD (Smith et al., 2010; Lossow et al., 2012; Lubi et al., 2016). Long-term changes in upper stratospheric ozone of up to -8% per decade derived from satellite measurements (e.g., Sofieva et al., 2017; WMO, 2018) could also affect the mesospheric circulation in the stratosphere and mesosphere by modulating the GW amplitudes and, hence, the GWD. Based on the

455 idealized approach of the present paper, we estimate the sensitivity of the amplification of the GW amplitudes in the upper mesosphere on changes in the ozone background μ_0 and the ozone-related heating rate $Q_0(\mu_0)$, revealing that, for horizontal and vertical wavelengths $L_k \geq 500$ km and $L_m \leq 5$ km, a change of $\pm 10\%$ in μ_0 or Q_0 results in a change of $\pm 10\%$ to $\pm 20\%$ in the upper mesospheric GWPED. Conclusively, the summer mesospheric upwelling might be much more sensitive to the long-term changes in upper stratospheric ozone as has been suggested by the GCMs up to now.



460 The results of the present paper might also stimulate further daytime-nighttime observations of GW activity particularly at specific measurement sites where the GWs are usually characterized by specific horizontal and vertical wavelengths, e.g., downwind of specific mountain ridges (east of Rocky Mountains, Southern Andes or Norwegian Caledonides), which could be helpful to better understand of how ozone-gravity wave coupling is operating in situ.

465 **Data Availability**

Background data and programs visualizing the presented analytic solutions are available at the IAP archive under <ftp://ftp.iap-kborn.de/data-in-publications/Gabriel/ACP2021/>.

Acknowledgment.

470 The author thanks Hauke Schmidt (MPI-Met, Hamburg) for providing HAMMONIA model data, and the German Climate Computing Center (DKRZ, Hamburg) for providing computer resources.

References

- Albers, J. R., McCormack, J. P. and Nathan, T. R.: Stratospheric ozone and the morphology of the northern hemisphere planetary waveguide, *J. Geophys. Res. Atmos.*, 118, 563–576, doi:10.1029/2012JD017937, 2013.
- 475 Alexander, M. J.: Interpretations of observed climatological patterns in stratospheric gravity wave variance, *J. Geophys. Res.*, 103, 8627–8640, 1998.
- Alexander, M. J. and Holton, J. R.: On the spectrum of vertically propagating gravity waves generated by a transient heat source, *Atmos. Chem. Phys.*, 4, 923–932, 2004.
- 480 Andrews, D. G., Holton, J. R. and Leovy, C. B.: *Middle Atmosphere Dynamics*. 489 pp., Academic Press, San Diego, California, 1987.
- Baumgarten, K., Gerding, M. and Lübken, F.-J.: Seasonal variation of gravity wave parameters using different filter methods with daylight lidar measurements at midlatitudes, *J. Geophys. Res. Atmos.*, 122, 2683–2695, doi:10.1002/2016JD025916, 2017.
- 485 Baumgarten, K., Gerding, M., Baumgarten, G. and Lübken, F.-J.: Temporal variability of tidal and gravity waves during a record long 10-day continuous lidar sounding, *Atmos. Chem. Phys.*, 18, 371–384, doi:10.5194/acp-18-371-2018, 2018.
- Brasseur, G. and Solomon, S.: *Aeronomy of the Middle Atmosphere*, D. Reidel Publishing Company, Dordrecht (Netherlands), 445 pages, 1995.



- Cariolle, D. and Morcrette, J.-J.: A linearized approach to the radiative budget of the stratosphere: influence of the ozone distribution, *Geophys. Res. Lett.*, 33, L05806, doi:10.1029/2005GL025597, 2006.
- 490 Chen, D., Strube, C., Ern, M., Preusse, P. and Riese, M.: Global analysis for periodic variations in gravity wave squared amplitudes and momentum fluxes in the middle atmosphere. *Ann. Geophys.*, 37, 487–506, doi.org/10.5194/angeo-37-487-2019, 2019.
- Cordero, E. C., Nathan, T. R. and Echols, R. S.: An analytical study of ozone feedbacks on Kelvin and Rossby-gravity waves: Effects on the QBO. *J. Atmos. Sci.*, 55, 1051–1062, 1998.
- 495 Cordero, E. C., and Nathan, T. R.: The Influence of Wave- and Zonal Mean-Ozone Feedbacks on the Quasi-biennial Oscillation, *J. Atmos. Sci.*, 57, 3426-3442, 2000.
- Dickinson, R. E.: Method of parameterization for infrared cooling between the altitude of 30 and 70 km. *J. Geophys. Res.*, 78, pp. 4451, 1973.
- 500 Douglass, A. R., Rood, R. B. and Stolarski, R. S.: Interpretation of Ozone Temperature Correlations 2. Analysis of SBUV Ozone Data, *J. Geophys. Res.*, 90(D6), 10, 693–10, 708, 1985.
- Ern, M., Preusse, P., Alexander, M. J. and Warner, C. D.: Absolute values of gravity wave momentum flux derived from satellite data, *J. Geophys. Res.*, 109, D20103, doi:10.1029/2004JD004752, 2004.
- Fritts, D. C., and Alexander, M. J.: Gravity wave dynamics and effects in the middle atmosphere, *Rev. Geophys.*, 41(1), 1003, doi:10.1029/2001RG000106, 2003.
- 505 Froidevaux, L., Allen, M., Berman, S. and Daughton, A.: The Mean Ozone Profile and Its Temperature Sensitivity in the Upper Stratosphere and Lower Mesosphere: An Analysis of LIMS Observations, *J. Geophys. Res.*, 94(D5), 6389–6417, 1989.
- Gabriel, A., Peters, D. H. W., Kirchner, I. and Graf, H.-F.: Effect of zonally asymmetric ozone on stratospheric temperature and planetary wave propagation. *GRL* 34, L06807, doi:10.1029/2006GL028998, 2007.
- 510 Gabriel, A., Körnich, H., Lossow, S., Peters, D. H. W., Urban, J., and Murtagh, D.: Zonal asymmetries in middle atmospheric ozone and water vapour derived from Odin satellite data 2001–2010, *Atmos. Chem. Phys.*, 11, 9865-9885, doi:10.5194/acp-11-9865-2011, 2011a.
- Gabriel, A., Schmidt, H. und Peters, D. H. W.: Effects of the 11-year solar cycle on middle atmospheric stationary wave patterns in temperature, ozone, and water vapor, *J. Geophys. Res.*, D23301, doi:10.1029/2011JD015825, 2011b.
- 515 Garcia, R. R., Smith, A., Kinnison, D., de La Cámara, Á. and Murphy, D. J.: Modification of the Gravity Wave Parameterization in the Whole Atmosphere Community Climate Model: Motivation and Results, *J. Atmos. Sci.*, 74, 275-291, doi:10.1175/JAS-D-16-0104.1, 2017.
- Gille, J. C. and Lyjak, L. V.: Radiative Heating and Cooling Rates in the Middle Atmosphere, *J. Atmos. Sci.*, 43, 2215-2229, 1986.
- 520 Gillett, N. P., Scinocca, J. F., Plummer, D. A. and Reader, M. C.: Sensitivity of climate to dynamically-consistent zonal asymmetries in ozone, *Geophys. Res. Lett.*, 36, L10809, doi:10.1029/2009GL037246, 2009.

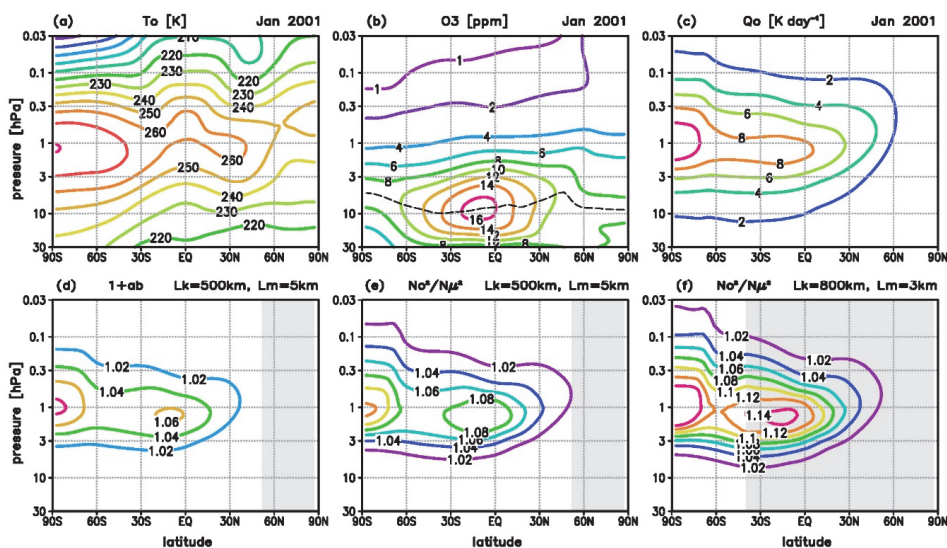


- Hocke, K., Lainer, M., Moreira, L., Hagen, J., Fernandez Vidal, S., and Schranz, F.: Atmospheric inertia-gravity waves retrieved from level-2 data of the satellite microwave limb sounder Aura/MLS, *Ann. Geophys.*, **34**, 781–788, doi:10.5194/angeo-34-781-2016, 2016.
- 525 Kaifler, B., Lübken, F.-J., Höffner, J., Morris, R. J. and Viehl, T. P.: Lidar observations of gravity wave activity in the middle atmosphere over Davis (69°S, 78°E), Antarctica, *J. Geophys. Res. Atmos.*, **120**, 4506–4521, doi:10.1002/2014JD022879, 2015.
- Lossow, S., McLandress, C. and Shepherd, T. G.: Influence of the Antarctic ozone hole on the polar mesopause region as simulated by the Canadian Middle Atmosphere Model. *J. Atmos. Sol. Terr. Phys.*, **74**, pp. 111-123, doi:10.1016/j.jastp.2011.10.010, 2012.
- Lubis, S. W., Omrani, N.-E., Matthes, K. and Wahl, S.: Impact of the Antarctic Ozone Hole on the Vertical Coupling of the Stratosphere–Mesosphere–Lower Thermosphere System, *J. Atmos. Sci.*, **73**, 2509-2528, doi:10.1175/JAS-D-15-0189.1, 2016.
- 535 McCormack, J. P., Nathan, T. R. and Cordero, E. C.: The effect of zonally asymmetric ozone heating on the Northern Hemisphere winter polar stratosphere, *Geophys. Res. Lett.*, **38**, L03802, doi:10.1029/2010GL045937, 2011.
- McLandress, C.: On the importance of gravity waves in the middle atmosphere and their parameterization in general circulation models. *J. Atmos. Sol. Terr. Phys.* **60**: 1357–1383, 1998.
- McLandress, C., Alexander, M. J. and Wu, D. L.: Microwave Limb Sounder observations of gravity waves in the stratosphere: A climatology and interpretation, *J. Geophys. Res.*, **105**, 11947–11967, 2000.
- 540 Nathan, T., R., and Cordero, E. C.: An ozone-modified refractive index for vertically propagating planetary waves, *J. Geophys. Res.*, **112**, D02105, doi:10.1029/2006JD007357, 2007.
- Schmidt, H., Brasseur, G. P. and Giorgetta, M. A.: Solar cycle signal in a general circulation and chemistry model with internally generated quasi-biennial oscillation, *J. Geophys. Res.*, **115**, D00I14, doi:10.1029/2009JD012542, 2010.
- 545 Smith, A., Garcia, R. R. Marsh, D. R., Kinnison, D. E. and J. H. Richter, J. H.: Simulations of the response of mesospheric circulation and temperature to the Antarctic ozone hole. *Geophys. Res. Lett.*, **37**, L22803, doi:10.1029/2010GL045255, 2010.
- Sofieva, V. F., Kyrölä, E., Laine, M., Tamminen, J., Degenstein, D., Bourassa, A., Roth, C., Zawada, D., Weber, M., Rozanov, A., Rahpoe, N., Stiller, G., Laeng, A., von Clarmann, T., Walker, K. A., Sheese, P., Hubert, D., van Roozendael, M., Zehner, C., Damadeo, R., Zawodny, J., Kramarova, N., and Bhartia, P. K.: Merged SAGE II, Ozone_cci and OMPS ozone profile dataset and evaluation of ozone trends in the stratosphere, *Atmos. Chem. Phys.*, **17**, 12533–12552, https://doi.org/10.5194/acp-17-12533-2017, 2017.
- 550 Ward, W. E., Oberheide, J., Riese, M., Preusse, P. and Offermann, D.: Planetary wave two signatures in CRISTA 2 ozone and temperature data, in *Atmospheric Science Across the Stratopause*, edited by D. E. Siskind, S. D. Eckermann and M. E. Summers, pp. 319-325, 2000.



Waugh, D. W., Oman, L., Newman, P. A., Stolarski, R. S., Pawson, S., Nielsen, J. E. and Perlwitz, J.: Effect of zonal asymmetries in stratospheric ozone on simulated Southern Hemisphere climate trends, *Geophys. Res. Lett.*, 36, L18701, doi:10.1029/2009GL040419, 2009.

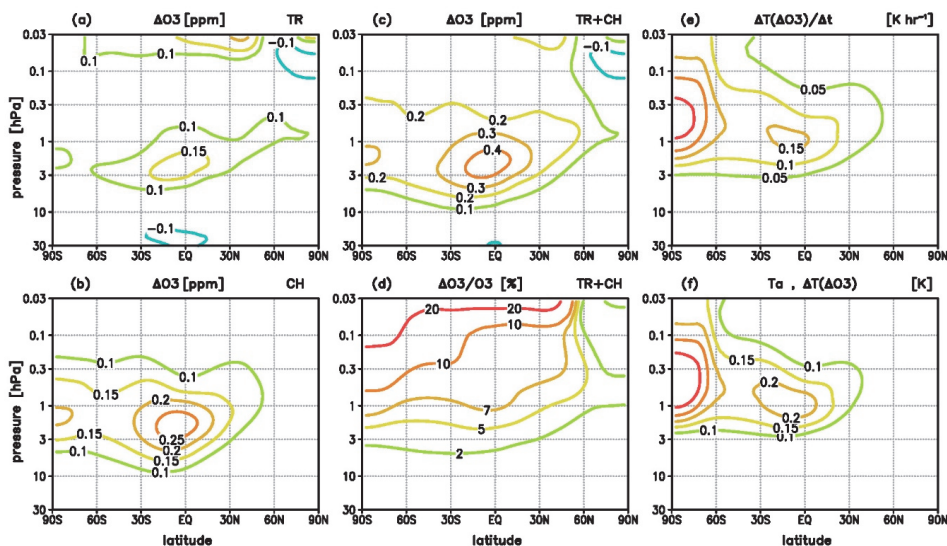
WMO (World Meteorological Organization): *Scientific Assessment of Ozone Depletion: 2018*, Global Ozone Research and Monitoring Project—Report No. 58, 588 pp., Geneva, Switzerland, 2018.



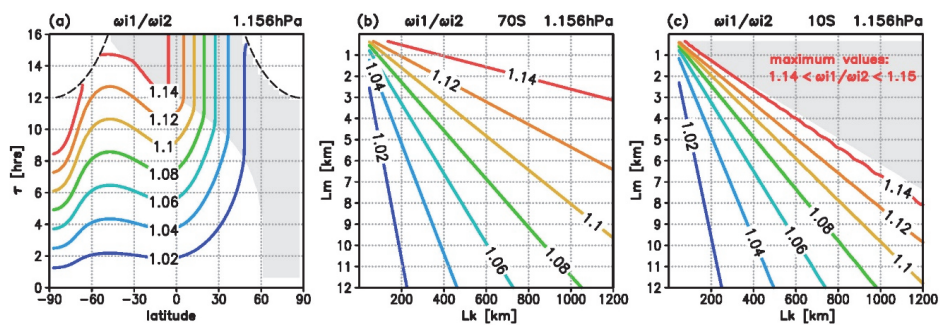
565

Figure 1: (a-c) Zonal and monthly mean background, (a) temperature T_0 , (b) ozone mixing ratio O_3 (the dashed line denotes where $\partial O_3 / \partial z = 0$) and (c) ozone heating rate Q_0 , January 2001, extracted from a simulation with the circulation and chemistry model HAMMONIA; (d-f) amplification factors (d) $1+ab$ and (e) N_0^2/N_{μ}^2 for a GW with horizontal and vertical wavelengths $L_k=500 \text{ km}$ and $L_m=5 \text{ km}$, and (f) N_0^2/N_{μ}^2 for a GW with $L_k=800 \text{ km}$ and $L_m=3 \text{ km}$; shaded areas denote the latitudes where the amplification is limited by the length of daylight ($\tau_i > \tau_{\text{day}}$).

570



575 **Figure 2:** Local changes due to ozone-temperature coupling induced by an initial GW perturbation with horizontal and vertical wavelengths $L_h=500$ km and $L_m=5$ km, and with exponential increase in amplitude with height ($\sim \exp^{-(z-z_s)/2H}$, initial temperature amplitude $T_a(z_s)=1$ K at $z_s \approx 35$ km ($p=6.28$ hPa)); (a) change in ozone due to vertical transport, (b) change in ozone due to photochemistry, (c) total change in ozone, (d) relative change in ozone, (e) change in the heating rate, (f) change in the temperature perturbation.



580

Figure 3: Amplification factor ω_1/ω_2 at a level of the maximum values of ω_1/ω_2 (1.156 hPa) illustrating the decrease of the intrinsic frequency with (ω_2) compared to without (ω_1) ozone-temperature coupling (compare with Figure 1e-f), (a) latitudinal distribution of ω_1/ω_2 as a function of the initial wave period τ_i [in hours], and (b-c) dependence of ω_1/ω_2 on the horizontal and vertical wavelengths L_k and L_m [in km] at (b) 70° S and (c) 10° S; shaded areas denote where the amplification is limited by the length of daylight ($\tau_i > \tau_{\text{day}}$).

585

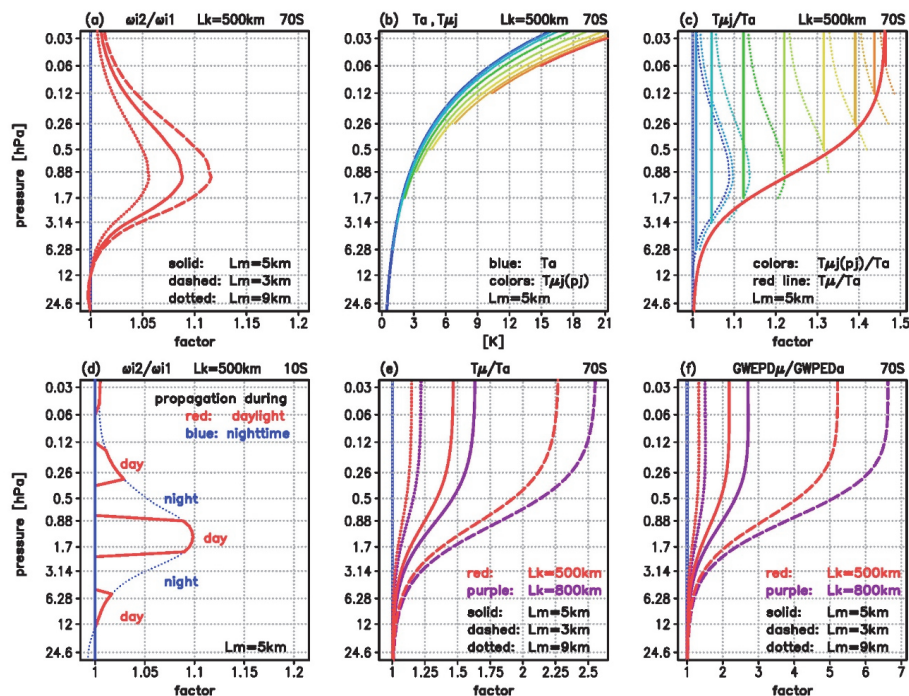
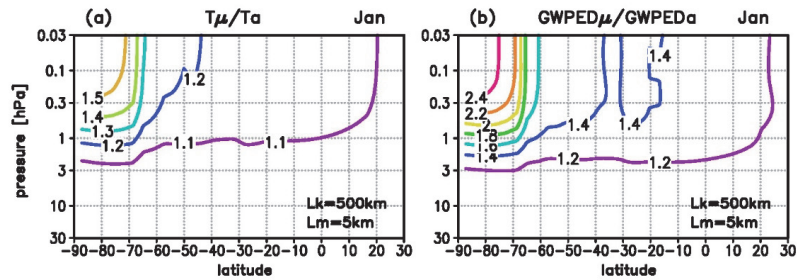


Figure 4: Illustration of the successive amplification of GW amplitudes during the upward level-by-level propagation, (a) amplification factor ω_{i2}/ω_{i1} at 70° S for a GW with horizontal wavelength $L_k=500$ km and vertical wavelength $L_m=5$ km (red solid line), and, for comparison, $L_m=3$ km (dashed) and $L_m=9$ km (dotted); (b) temperature amplitudes for the GW with $L_k=500$ km and $L_m=5$ km, depicting the initial perturbation T_a (blue) and the successively amplified amplitudes $T_{\mu j}(z_j)_{j=1..n}$ (light blue towards red; here, $n=8$ for $L_m=5$ km), (c) same as (b) but for the relative amplitudes $T_{\mu j}(z_j)/T_a$ (solid lines) together with the profiles of the previous level multiplied by ω_{i1}/ω_{i2} (i.e., $T_{\mu j-1}(z_{j-1}) \cdot (\omega_{i1}/\omega_{i2})$), dashed lines) and a fitted approach T_μ (thick red solid line, defined by Eq. 18), (d) same as (a) for the case $L_k=500$ km and $L_m=5$ km but at 10° S including the limitation due to the length of night-time conditions, (e) relative values T_μ/T_a at 70° S for different horizontal (red: $L_k=500$ km, purple: $L_k=800$ km) and vertical (dashed: $L_m=3$ km, solid: $L_m=5$ km, dotted: $L_m=9$ km) wavelengths, (f) same as (e) but for the relative values E_μ/E_a of the related gravity wave potential energy density (GWPED, defined by Eq. 19).



600 **Figure 5:** Cumulative amplification of the GW amplitude during the upward level-by-level propagation for a GW with $L_k=500$ km and $L_m=5$ km, (a) cumulative increase in the temperature amplitudes described by $T\mu/T\alpha$, (b) related increase in the gravity wave potential energy density (GWPED) described by $E\mu/E\alpha$; background conditions: January 2001.



605

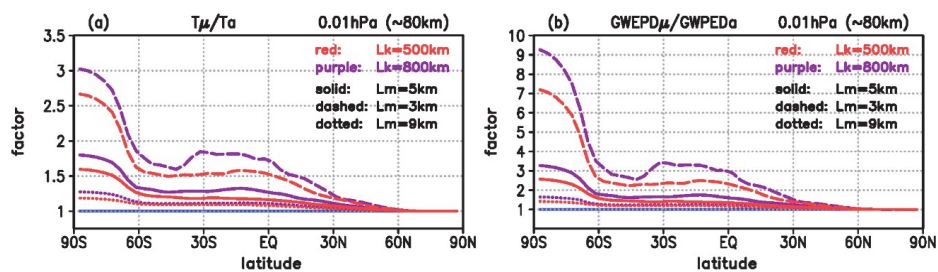


Figure 6: Cumulative amplification of the GW amplitudes similar as in Figure 5 but at upper mesospheric levels (0.01 hPa, ~80 km) for different horizontal and vertical wavelengths L_k (red: 500 km, purple: 800 km) and L_m (dotted: 9 km, solid: 5 km, dashed: 3 km), (a) T_μ/T_a , (b) E_μ/E_a .